J Electroceram (2006) 16:399–402
DOI 10.1007/s10832-006-9887-z

Surface potential properties on near-stoichiometric $LiNbO_3$ crystals with nanoscale domain-engineered structures

Xiaoyan Liu · Kazuya Terabe · Kenji Kitamura

Abstract We studied the surface potential properties of nanoscale domain-engineered structures on near-stoichiometric $LiNbO_3$ crystals using Kelvin probe-based, electrostatic force microscopy. The surface potential image reflected in the domain structures could not be obtained clearly, because the spontaneous polarizations of the domains were neutralized by the in-air room temperature (298 K) screening charges. However, using heat-treatment in a vacuum, the surface potential image became clear, because of the decrease of the spontaneous polarizations and the protection of the screening charge adsorption. Furthermore, the surface potential contrast and polarity of the nanoscale domain-engineered structures could be changed repeatedly by changing the temperature between 298 and 393 K in the vacuum.

Keywords Near-stoichiometric $LiNbO_3$ · Surface potential · Spontaneous polarization · Pyroelectric properties · EFM

1 Introduction

Ferroelectric materials, such as $LiNbO_3$ and $LiTaO_3$ crystals, are of considerable interest for applications in electron acceleration and the accompanying bremsstrahlung radiation systems [1], micro-electro-mechanical systems (MEMS) [2], and thermal infrared detectors [3], because of their unique pyroelectric properties associated with spontaneous polarization. If optional control of the spontaneous polarization distribution in the microscale to nanoscale range can be realized, it will be possible to improve the performance of these applications and create new function devices and templates.

Recently, a scanning force microscope (SFM) was successfully used to perform microscale to nanoscale domain engineering in ferroelectric materials, such as $LiNbO_3$ crystals [4–6]. In addition, electrostatic force microscopy (EFM) has become a powerful tool for characterizing the surface potential distribution of ferroelectric domain structures [7, 8]. On the other hand, a new crystal growth technique called double-crucible Czochralski [9] has been developed to grow near-stoichiometric $LiNbO_3$ (SLN) crystals with low non-stoichiometric defect density. Compared with conventional congruent $LiNbO_3$ single crystals, SLN crystals have lower coercive field (an electric field required for domain inversion), and enable us to engineer high quality nano-domain structures using SFM [10].

Up to now, the temperature and time dependent behavior of surface potential in air of naturally formed micro-domain structures has been reported in $BaTiO_3$ crystals [11, 12]. In this work, we investigated in-vacuum surface potential properties of nanoscale domain-engineered structures in the SLN crystals using EFM. The in-vacuum measurement allows obtain a clear surface potential contrast between the nanoscale inverted and original domains during the reverse heating and cooling processes. Moreover the screening process proceeded much slower in vacuum than that in air, then makes a possible to control of the contrast and polarity of surface potential with nanoscale domain-engineered structures. By using the in-vacuum surface potential properties on SLN crystals, we furthermore demonstrated the controllability of the surface potential contrast and polarity with nanoscale domain-engineered structures.

X. Liu (✉) · K. Terabe · K. Kitamura
National Institute for Materials Science, 1-1 Namiki, Tsukuba, 305-0044, Japan
e-mail: liu.xiaoyan@mims.go.jp

X. Liu · K. Kitamura
Interdisciplinary Graduate School of Engineering Sciences
Kyushu University, 6-1, Kasuga-Koen, Kasuga, 816-8580, Japan

2 Experiments

The SLN single crystals were grown using the double-crucible Czochralski technique [9]. The crystal, which had a single 180°-domain structure, was cut perpendicular to the Z-axis, and an indium tin oxide (ITO) electrode was deposited on the +Z surface of the sample by magnetron sputtering. The SLN sample was mounted with its −Z surface facing up on the 0.5-mm-thick congruent $LiNbO_3$ substrate using an organic adhesive, and then polished to a thickness of 800 nm. Conductive silver paste was used to set the sample on an SFM stage and establish electrical contact between the ITO electrode and the stage. Domain engineering was performed by applying a dc bias voltage to the –Z surface of the sample through a conductive cantilever of SFM [4–6]. A rhodium-coated silicon cantilever with spring constants of 2.1 N/m and a resonance frequency of 29 kHz was used for domain engineering and the following surface potential measurements:

First, we measured the surface potential distribution of nanoscale domain-engineered structures using a Kelvin probe-based EFM at room temperature in air. Then, the sample system was vacuumed for over 10 h to establish a constant vacuum of about 7.5×10^{-7} Torr. A heat-treatment in which the temperature was increased from 298 to 393 K was performed after vacuuming. The temperature dependence of the surface potential contrast was investigated in the vacuum as the heating and cooling processes were reversed twice, at intervals of 298 to 393 K. The surface potential was measured after holding the sample for 30 min. at each temperature. Furthermore, we demonstrated the time dependence of the surface potential contrast by maintaining the sample at room temperature in the vacuum. All the surface potential measurements were performed in the same nanoscale domain-engineered structure location.

3 Results and discussion

The structure of the linearly engineered domains in SLN crystals is shown in Fig. 1(a), which was imaged using piezoresponse force microscopy. The linear domains with +Z surfaces (black regions) are 800-nm wide and are separated by 8-μm spaces. The surface potential image obtained at room temperature in air is shown in Fig. 1(b). The surface potential contrast between the linear (+Z surface) and original domains (−Z surface) was very small (∼ 2 mV), thus the surface potential distribution was almost random. However, by heating the sample to 393 K in the vacuum, the surface potential contrast was clarified. Figure 2 shows the surface potential images of the linear domains during the in-vacuum cooling process at (a) 393 K, (b) 373 K, and (c) 363 K. The surface potential contrast between the linear domains and the original domains were –70 mV at 393 K, ∼ −10 mV at 373 K and +70 mV at 363 K. They indicate that the surface potential polarity of the linear domains inverted when the temperature changed from 393 to 363 K, i.e. a negative surface potential (black) became positive (white). Figure 2(b) shows that the inversion occurred at around 373 K.

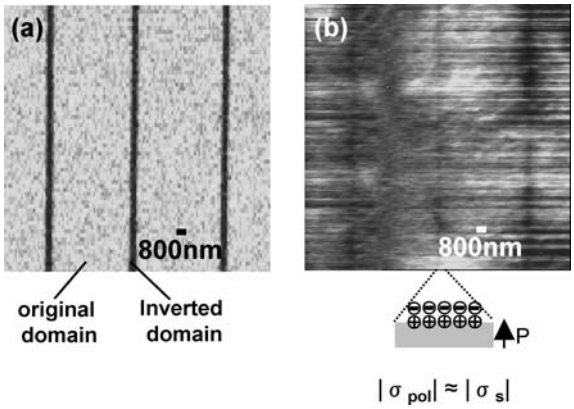

Fig. 1 Piezoresponse image (a) and surface potential image (b) of a linear domain structure in SLN crystals at room temperature in air. The schema shows the screened surface of the linear domains

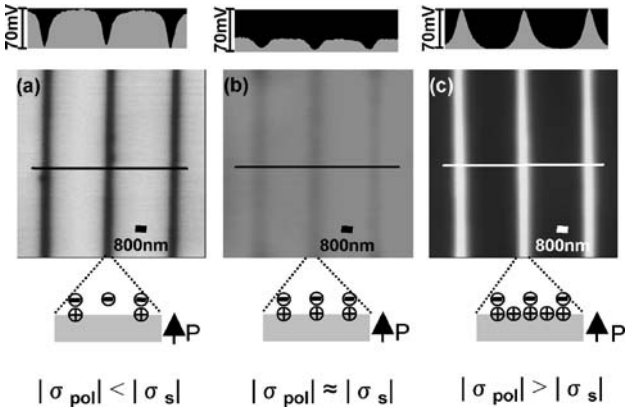

Fig. 2 Surface potential images of linear domain structure after heating to 393 K, and cooling from (a) 393 K to (b) 373 K, and (c) 363 K in the vacuum. The schemas show the changes in the surfaces of the linear domains. The surface potential distributions along the lines in figures (a) to (c) are also shown

The temperature dependence of the surface potential contrast at intervals of 298 to 393 K in the vacuum is shown in Fig. 3. We observed this repetitive behavior, in which the surface potential contrast changed linearly between ∼ −70 and ∼ 320 mV, as the temperature changed during the reverse heating and cooling processes. The surface potential polarity inversion point during the heating and cooling processes was estimated at 370 K. Furthermore, we demonstrated the time dependence of the surface potential contrast by maintaining the sample at room temperature in the vacuum, as illustrated in Fig. 4. This shows that the surface potential contrast remained constant for several hours, and then decreased slowly over time until the surface reached a neutralized state after 50 h.

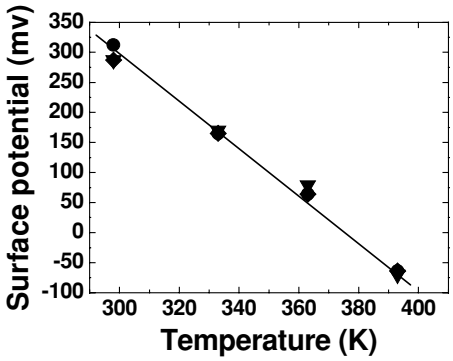

Fig. 3 Temperature dependence of surface potential contrast on cooling (▼), heating (♦) and re-cooling (•) at temperature intervals of 298 to 393 K in the vacuum. We observed this repeated behavior, in which the surface potential decreased as the temperature increased, during the reverse heating and cooling processes

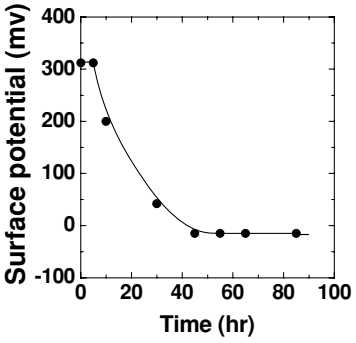

Fig. 4 Time dependence of surface potential contrast at room temperature in the vacuum. Measurements were performed by maintaining the sample at room temperature in the vacuum after measuring the temperature dependence of the surface potential contrast

In the unscreened state, the ferroelectric material surface is characterized by a spontaneous polarization charge density $\sigma_{\mathbf{pol}} = \mathbf{P} \cdot \mathbf{n}$, where $\mathbf{P}$ is the polarization vector and $\mathbf{n}$ is the unit normal to the surface. However, the unscreened state is unstable, and polarization charges are always screened by the surface adsorption of the charged ions or particles from the environment [13]. The surface layer is represented by the polarization (σ_{pol}) and the screening charges (σ_s), which are opposite polarities. Screening charges are supposed to be very complex in accumulation layers. In room temperature air, the polarization charges are completely screened ($|\sigma_{pol}| = |\sigma_s|$) by the surface adsorption, and thus the surface potential reveals a neutralized state, as shown in Fig. 1(b). By heating the sample to 393 K in the vacuum, the screening charges on the sample surface decreased gradually, but were not completely removed because of the relatively low heating temperature. After the heat-treatment, the screening charges were supposed to remain almost constant for several hours because of the slow screening process in the vacuum (Fig. 4). However, the spontaneous polarization charges decrease as the temperature increased due to the pyroelectric effect. Therefore, the surface potential, which is significantly effected by the screening and the spontaneous polarization charges, changed with the temperature in the vacuum. The screening charges were predominant on the high temperature surface, while the polarization charges were predominant on the low temperature surface. Using the cooling process shown in Fig. 2 as an example, the surface potential showed signs of screening charges because the screening charges exceeded the polarization charges ($|\sigma_{pol}| < |\sigma_s|$) at high temperatures (393 K, Fig. 2(a)). Decreasing the temperature increases the polarization charges, thus neutralizing the excess screening charges (Fig. 2(b)). With temperatures below 373 K, the polarization charges exceed the screening charges ($|\sigma_{\mathbf{pol}}| > |\sigma_s|$), thus inducing the surface potential to invert (Fig. 2(c)). Also, conserving the screening charges in the vacuum leads to repeatable linear changes in the surface potential during the reverse cooling and heating processes (Fig. 3). Actually, after the conservation period the screening charges increased slowly over time until finally, 50-h later, they neutralized the polarization charges (Fig. 4) because of the imperfect vacuum conditions. *Kalinin* et al. reported the surface potential behavior of ferroelectric $BaTiO_3$ crystals in air [11, 12]. Our results are consistent with theirs. The in-vacuum screening process proceeded much more slowly than that in air. The slower screening process in the vacuum allows control of the surface potential contrast and the polarity of nanoscale domain-engineered structures in the SLN crystals.

The controllability of the surface potential contrast and polarity of nanoscale domain structures were demonstrated on the –Z surface of SLN crystal by writing domains to form the character "NIMS" as shown in Fig. 5. The in-vacuum heat-treatment described as above was carried out after the engineering and imaging of the domain word. The piezoresponse image of the word with the domain width of 300 nm is shown in Fig. 5(a) while its surface potential images during the cooling process in the vacuum at 393 K and 333 K are shown in Fig. (b) and (c). It is clear that, the surface potential polarity of the character "NIMS" domain was inverted completely by changing the temperature in vacuum.

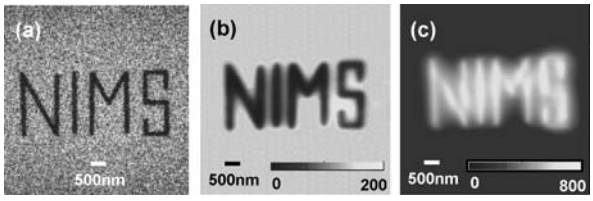

Fig. 5 The character formed by nanoscale domains engineered on the −Z surface of SLN crystal. (a) piezoresponse image of the character, surface potential images of the character after heating to 393 K, and cooling from (b) 393 K to (c) 333 K in the vacuum

The optional control of the surface potential contrast and polarity in a required nanoscale domain structure could be realized by using the surface potential properties on the SLN crystals.

4 Conclusions

We studied the surface potential properties of SLN crystals with nanoscale domain-engineered structures at temperature intervals of 298 to 393 K using Kelvin probe-based EFM. After heat-treatment, the screening charges remained constant for several hours, due to the protection from surface adsorption in the vacuum. The conservation of the screening charges in the vacuum resulted in repeatable linear changes in the surface potential within the temperature range, depending on the spontaneous polarization charges. These results verify the feasibility of controlling the surface potential contrast and polarity in a microscale to nanoscale range using the nanoscale domain-engineered structures in the SLN crystals.

References

1. B. Naranjo, J.K. Gimzewski, and S. Putterman, *Nature*, **434**, 1115 (2005).
2. D.L. Polla and L.F. Francis, *Annu. Rew. Mater. Sci.,* **28**, 563 (1998).
3. P. Muralt, *Rep. Prog. Phys*., **64**, 1339 (2001).
4. K. Terabe, M. Nakamura, S. Takegawa, K. Kitamura, S. Higuchi, Y. Gotoh, and Y. Cho, *Appl. Phys. Lett.,* **82**, 433 (2003).
5. K. Terabe, X.Y. Liu, M. Nakamura, S. Takegawa, and K. Kitamura, *Mater. Tech.,* **19**, 162 (2004).
6. B.J. Rodriguez, R.J. Nemanich, A. Kingon, A. Gruverman, S.V. Kalinin, K. Terabe, X. Y. Liu, and K. Kitamura, *Appl. Phys. Lett.,* **86**, 012906 (2005).
7. H. Bluhm, A. Wadas, R. Wiesendanger, A. Roshko, J.A. Aust, and D. Nam, *Appl. Phys. Lett.,* **71**(1), 146 (1997).
8. S. Tsunekawa, J. Ichikawa, H. Nagata, and T. Fukuda, *Appl. Surf. Sci.,* **137**, 61 (1999).
9. K. Kitamura, J.K. Yamamoto, N. Iyi, S. Kimura, and T. Hayashi, *J. Cryst. Growth*, **116**, 327 (1992).
10. X.Y. Liu, K. Terabe, and K. Kitamura, *Jpn. J. Appl. Phys.,* **44**, 7012 (2005).
11. S.V. Kalinin and D.A. Bonnell, *Appl. Phys. Lett.,* **78**, 1116 (2001).
12. S.V. Kalinin, C.Y. Johnson, and D.A. Bonnell, *J. Appl. Phys.,* **91**, 3816 (2002).
13. V.M. Fridkin, *Ferroelectric Semiconductors* (Consultants Bureau, New York, 1980).